

The APOSTLE simulations: Rotation curves derived from synthetic 21-cm observations

Kyle A. Oman¹

¹Department of Physics and Astronomy, University of Victoria,
Victoria, BC V8P 5C2, Canada
email: koman@uvic.ca

Abstract. The APOSTLE cosmological hydrodynamical simulation suite is a collection of twelve regions ~ 5 Mpc in diameter, selected to resemble the Local Group of galaxies in terms of kinematics and environment, and re-simulated at high resolution (minimum gas particle mass of $10^4 M_\odot$) using the galaxy formation model and calibration developed for the EAGLE project. I select a sample of dwarf galaxies ($60 < V_{\max}/\text{km s}^{-1} < 120$) from these simulations and construct synthetic spatially- and spectrally-resolved observations of their 21-cm emission. Using the ^{3D}BAROLO tilted-ring modelling tool, I extract rotation curves from the synthetic data cubes. In many cases, non-circular motions present in the gas disc hinder the recovery of a rotation curve which accurately traces the underlying mass distribution; a large central deficit of dark matter, relative to the predictions of cold dark matter N-body simulations, may then be erroneously inferred.

Keywords. Galaxies: halos, galaxies: kinematics and dynamics, dark matter

1. Introduction

1.1. The APOSTLE simulation suite

The APOSTLE[†] simulation suite (Fattahi *et al.*, 2016a; Sawala *et al.*, 2016) is a collection of fully cosmological hydrodynamical simulations of 12 regions each approximately 5 Mpc in diameter. These are selected from a large cosmological N-body simulation to resemble the Local Group of galaxies in terms of the properties of the two most massive objects, analogous to the Milky Way (MW) and M 31, in terms of their virial masses, approach and tangential velocity, recession velocity of surrounding objects, and isolation from more massive structures. Each region is re-simulated at multiple resolution levels (see Table 1) using the modified P-GADGET3 smoothed-particle hydrodynamics code and calibrated galaxy formation model developed for the EAGLE project (specifically, the model is the one denoted ‘Ref’ by Schaye *et al.*, 2015; see also Crain *et al.*, 2015). At present, 5 of the simulation volumes have been evolved at L1 resolution; all 12 volumes have been evolved at L2 and L3 resolution.

[†] A Project Of Simulating The Local Environment.

Table 1. Particle masses and force softening for the three APOSTLE resolution levels, denoted AP-L3 (lowest) to AP-L1 (highest).

Resolution level	DM particle ¹ mass [M_\odot]	Gas particle mass [M_\odot]	Force softening [pc]
AP-L3	7.3×10^6	1.5×10^6	711
AP-L2	5.9×10^5	1.3×10^5	307
AP-L1	5.0×10^4	1.0×10^4	134

Notes:

¹Particle masses vary by up to a factor of 2 from volume to volume; values given are indicative.

The EAGLE model is calibrated to reproduce the $z = 0.1$ galaxy stellar mass function (GSMF) and galaxy size distribution across the range $10^8 < M_*/M_\odot < 10^{11}$. The APOSTLE suite demonstrates that the same model, without recalibration, reproduces on average the Local Group GSMF down to $M_* = 10^5 M_\odot$ (Sawala *et al.*, 2016), and the size distribution down to $M_* = 3 \times 10^6 M_\odot$ (Campbell *et al.*, 2017). The APOSTLE MW and M 31 analogs do not suffer from the ‘too-big-to-fail’ problem, defined by Boylan-Kolchin *et al.* (2011): their satellite galaxies occupy dark matter halos consistent with the observed velocity dispersions of dwarf spheroidal galaxies in the Local Group (Sawala *et al.*, 2016; Fattahi *et al.*, 2016b).

The simulation suite has been used to assist studies of stellar disc dynamics (Yozin *et al.* in preparation), the structure of gaseous discs (Benítez-Llambay *et al.*, 2017), the assembly of stellar halos (Starkenburger *et al.*, 2017; Oman *et al.*, 2017b), the baryonic Tully-Fisher relation (Oman *et al.*, 2016; Sales *et al.*, 2017), the properties of low-mass, starless dark matter haloes (Benítez-Llambay *et al.*, 2016; Sawala *et al.*, 2017), the tidal stripping of satellite galaxies (Fattahi *et al.*, 2017; Wang *et al.*, 2017), the mass discrepancy – acceleration relation (Ludlow *et al.*, 2017; Navarro *et al.*, 2017), and the dark matter cusp-core problem (Oman *et al.*, 2015; 2017a; Genina *et al.*, 2017).

1.2. The dark matter cusp-core problem

N-body simulations generically predict that cold dark matter halos have radial density profiles which rise steeply toward the halo centre, with a logarithmic slope of ≈ -1 (Navarro *et al.*, 1996a; 1997), termed a cusp. The density profiles for some galaxies, as inferred from their rotation curves or other dynamical mass estimators, however, imply an approximately constant central dark matter density (slope ≈ 0) within some ‘core’ region (Moore 1994; Flores & Primack 1994; and see de Blok 2010 for a review). The same discrepancy can also be cast as a central deficit of mass, relative to the prediction from N-body simulations, as in Oman *et al.* (2015). An important constraint on any proposed solution to this problem is the diversity in the rotation curves of galaxies at fixed maximum rotation velocity V_{\max} , especially those of dwarfs of $30 \lesssim V_{\max}/\text{km s}^{-1} \lesssim 100$. Any mechanism proposed to create cores – or the appearance of a core – must do so in some galaxies and not in others, and to different extent in different galaxies.

Currently viable resolutions of the cusp-core problem can be summarized as falling into several categories (or combinations thereof):

- The dark matter distribution, presumed initially cuspy, may be modified by gravitational coupling to violent motions of gas within the galaxy (Navarro *et al.*, 1996b; Read & Gilmore, 2005; and for a review see Pontzen & Governato, 2014).
- If the dark matter physics differs from that of generic cold dark matter, for instance if the dark matter is warm (Bode *et al.*, 2001; Lovell *et al.*, 2012) or self-interacting (Spergel & Steinhardt, 2000; Creasey *et al.*, 2017), the density profile may be modified.
- Systematic effects and errors in the modelling of observed galaxies could cause the appearance of a core in a system hosting a dark matter cusp (Rhee *et al.*, 2004; Valenzuela *et al.*, 2007; Kuzio de Naray & Kaufmann, 2011; Read *et al.*, 2016; Pineda *et al.*, 2017; Oman *et al.*, 2017a; and references therein).

2. Method

2.1. Synthetic observations

I select the 33 galaxies from the APOSTLE L1 resolution simulations which lie in the interval $60 < V_{\max}/\text{kms}^{-1} < 120$. The upper bound ensures that the galaxies are ‘dark matter-dominated’ in the sense that when the gravitational force is decomposed into

contributions from dark matter and stars and gas, the component due to the dark matter is dominant, on average, at every radius. The lower bound ensures that corrections to the rotation curve to account for ‘pressure support’ (for a detailed discussion of such corrections see Valenzuela *et al.*, 2007; Pineda *et al.*, 2017) are usually small.

The HI distribution in each galaxy is computed from the particle positions, chemical compositions, temperatures and densities following the prescription of Rahmati *et al.* (2013) for self-shielding from the metagalactic ionizing background radiation, with a correction for the molecular gas fraction following Blitz & Rosolowsky (2006). Each galaxy is then ‘observed’ to produce a synthetic data cube, mimicking where possible the characteristics of the LITTLE THINGS HI survey (Hunter *et al.*, 2012). The galaxies are placed at a nominal distance of 3 Mpc and an inclination of 60° . Another angle, Φ , corresponding to an azimuthal rotation of the galaxy, needs to be chosen to specify a unique line of sight – this angle is randomly selected. The HI distribution is mapped onto a grid with a pixel spacing of 3 arcsec and convolved with a 6 arcsec gaussian beam. In the velocity direction, each particle contributes a gaussian line profile of 7 km s^{-1} fixed width, and amplitude proportional to the HI mass of the particle. In each pixel the velocity information is sampled in channels of 4 km s^{-1} width.

Fig. 1 is a visualization of one of the simulated galaxies, AP-L1-V1-8-0[†] seen from two viewing angles separated by 90° , at a fixed inclination of 60° . Note that, for illustrative purposes, the viewing angles have been carefully chosen, rather than randomized as described above. The maps show the intensity-weighted mean velocity in each pixel, and the straight lines indicate the kinematic major axis of each projection. Galaxies at this mass scale have substantial azimuthal asymmetries, reflected here as differences between the velocity fields after an azimuthal rotation.

2.2. Rotation curve modelling

Using the ^{3D}BAROLO tilted-ring modelling software (Di Teodoro & Fraternali, 2015), a rotation curve is extracted from each synthetic data cube. ^{3D}BAROLO does not model the velocity field, but rather constructs a full model data cube whose residual with respect to the observed data cube is minimized via an iterative variation of the parameters of each ‘ring’ in the model. The configuration used is as in Iorio *et al.* (2017), except where

[†] AP-[resolution level]-[volume number]-[friends-of-friends group number]-[subgroup number].

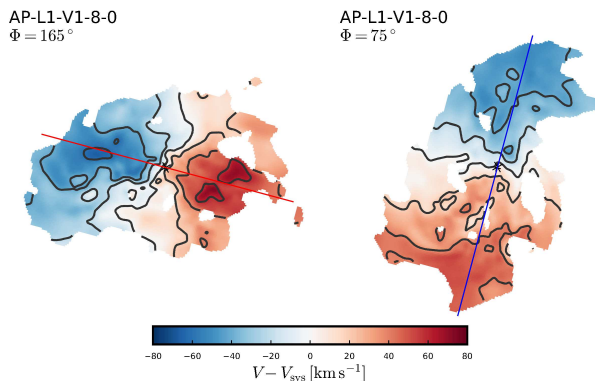


Figure 1. ‘Synthetically observed’ HI intensity-weighted mean velocity field for the simulated dwarf galaxy AP-L1-V1-8-0 viewed from two directions separated by 90° , at fixed inclination $i = 60^\circ$. The straight lines indicate the kinematic major axis of each projection. (Adapted from Oman *et al.* 2017, fig. 8.)

parameters need to be set on a per-galaxy basis (e.g. centroid, size, inclination, position angle). The centroid is fixed to the peak of the simulated stellar particle distribution as seen along the ‘line of sight’. The inclination and position angles are set to the known values used to construct the synthetic observations, but allowed to vary in the fitting process by up to 15° and 20° , respectively.

The rotation curves are corrected for pressure support as:

$$V_{\text{circ}}^2 = V_{\text{rot}}^2 - \sigma^2 \frac{d \log(\Sigma_{\text{HI}} \sigma^2)}{d \log R} \quad (2.1)$$

where V_{rot} is the rotation curve as recovered by ^3D BAROLO, V_{circ} is the corrected rotation curve, σ is the H I velocity dispersion and Σ_{HI} is the H I surface density – all these quantities are measured directly from the synthetic data cubes.

3. Results

The rotation curves for AP-L1-V1-8-0 corresponding to the two orientations shown in Fig. 1 are shown in Fig. 2 as coloured lines; the thicker lines are the pressure support-corrected versions of the rotation curves shown with thin lines. The gray lines show the rotation speed as a function of radius for the simulated H I gas as measured directly from the simulation output, i.e. without the added handicaps of projection, limited ‘observational resolution’, etc. Finally, the thick black line shows the circular velocity curve for this galaxy, computed as $V_{\text{circ}} = \sqrt{GM(< R)/R}$, where $M(< R)$ is the mass enclosed within radius R , and G is the gravitational constant. The dark matter is the dominant contributor to $M(< R)$ at all radii for all simulated galaxies in the sample. In the orientation labelled $\Phi = 165^\circ$, the ‘observed’ rotation curve overestimates somewhat the rotation speed of the gas in the galaxy; in the $\Phi = 75^\circ$ orientation, the rotation curve is *severely* underestimated.

The leading reason for the difference between the two rotation curves in Fig. 2 is the presence of a non-circular, bisymmetric flow pattern superimposed on the rotation. This imposes a velocity modulation which has two peaks and two troughs along an azimuthal loop around the galaxy. The rotation curve is driven up when gas rotating faster than

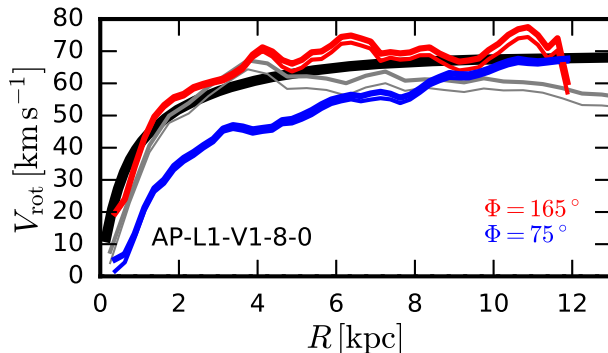


Figure 2. The thick black curve is the circular velocity profile of simulated galaxy AP-L1-V1-8-0 (the same object used in Fig. 1). The thin and thick gray lines indicate the rotation speed of H I gas in this galaxy as a function of radius, before and after correction for pressure support, respectively. The thin red and blue curves are the rotation curves obtained from a ^3D BAROLO modelling of the synthetic H I datacubes corresponding to the two orientations for which the velocity fields are shown in Fig. 1. The application of a correction for pressure support yields the thick red and blue curves. (Adapted from Oman *et al.* 2017, fig. 5.)

the average at that radius falls on the major axis of the galaxy in projection, and down when gas rotating more slowly falls there. Such features are common in the simulated sample and lead to a wide diversity of rotation curve shapes, this despite the fact that all retain their dark matter cusp and are dark matter dominated – if their rotation curves faithfully traced their circular velocity curves the shapes would all be self-similar.

Though such bisymmetric flow patterns are easily discerned based on the simulation particle properties, their signature in the synthetic observations is more subtle. In some cases where the rotation curve is severely underestimated, I have been unable to identify any clear indication that anything might be amiss; were these real galaxies, I might erroneously come to the conclusion that they host dark matter cores.

Considering the sample of 33 simulated galaxies as a whole, when each is modelled with a random orientation (at fixed inclination $i = 60^\circ$, see Sec. 2.1), the width of the rotation curve shape distribution, parametrized by the rotation speed at 2 kpc and V_{\max} (Oman *et al.*, 2015), is comparable to that seen in real galaxies (Oman *et al.*, 2017a).

4. Conclusions

The ability of the scenario outlined above to constitute a convincing resolution of the cusp-core problem hinges on the ‘realism’ of the simulated galaxies. The data cubes constructed for the APOSTLE dwarfs compare favourably with those from the THINGS (Walter *et al.*, 2008) and LITTLE THINGS (Hunter *et al.*, 2012) surveys according to several metrics (Oman *et al.*, 2017a), but there are some differences even at this rudimentary level of comparison: the APOSTLE galaxies have somewhat higher velocity dispersions on average, and perhaps also thicker HI discs. Nevertheless, there is some indication that bisymmetric non-circular flow patterns sufficiently strong to cause substantial changes to their rotation curves may be present in the DDO 47 and DDO 87 galaxies (Oman *et al.*, 2017a): the residuals after subtraction of a tilted-ring model from their velocity fields reveal a ‘trefoil’ shape characteristic of a bisymmetric distortion seen in projection. I urge continued strong caution when interpreting the rotation curves of dwarf galaxies, especially in the central regions which are often poorly sampled and in which the potential impact of errors due to non-circular motions is strongest.

References

- Benítez-Llambay, A., Navarro, J. F., Frenk, C. S., Sawala, T., Oman, K. A., Fattahi, A., Schaller, M., Schaye, J., *et al.* 2016, *MNRAS*, 465, 3913
- Benítez-Llambay, A., Navarro, J. F., Frenk, C. S., & Ludlow, A. D. 2017, *pre-print*, arXiv: 1707.08046
- Boylan-Kolchin, M., Bullock, J. S., & Kaplinghat, M. 2011, *MNRAS*, 415, 40
- Bode, P., Ostriker, J. P., & Turok, N. 2001, *ApJ*, 556, 93
- Campbell, D. J. R., Frenk, C. S., Jenkins, A., Eke, V. R., Navarro, J. F., Sawala, T., Schaller, M., Fattahi, A., *et al.* 2017, *MNRAS*, 469, 2335
- Crain, R. A., Schaye, J., Bower, R. G., Furlong, M., Schaller, M., Theuns, T., Dalla Vecchia, C., Frenk, C. S., *et al.* 2015, *MNRAS*, 450, 1937
- Creasey, P., Sameie, O., Sales, L. V., Yu, H.-B., Vogelsberger, M., & Zavala, J. 2017, *MNRAS*, 468, 2283
- de Blok, W. J. G. 2010, *Advances in Astronomy*, 2010, 789293
- Di Teodoro, E. M., & Fraternali, F. 2015, *MNRAS*, 451, 3021
- Fattahi, A., Navarro, J. F., Sawala, T., Frenk, C. S., Oman, K. A., Crain, R. A., Furlong, M., Schaller, M., *et al.* 2016a, *MNRAS*, 457, 844
- Fattahi, A., Navarro, J. F., Sawala, T., Frenk, C. S., Sales, L. V., Oman, K. A., Schaller, M., & Wang, J. 2016b, *pre-print*, arXiv: 1607.06479

- Fattahi, A., Navarro, J. F., Frenk, C. S., Oman, K. A., Sawala, T., & Schaller, M. 2017, *pre-print*, arXiv: 1707.03898
- Flores, R. A., & Primack, J. R. 1994, *ApJ*, 427, L1
- Genina, A., Benítez-Llambay, A., Frenk, C. S., Cole, S., Fattahi, A., Navarro, J. F., Oman, K. A., Sawala, T., *et al.* 2017, *pre-print*, arXiv: 1707.06303
- Hunter, D. A., Ficut-Vicas, D., Ashley, T., Brinks, E., Cigan, P., Elmegreen, B. G., Heesen, V., Herrmann, K. A., *et al.* 2012, *AJ*, 144, 134
- Iorio, G., Fraternali, F., Nipoti, C., Di Teodoro, E., Read, J. I., & Battaglia, G. 2017, *MNRAS*, 466, 4159
- Kuzio de Naray, R., & Kaufmann, T. 2011, *MNRAS*, 414, 3617
- Lovell, M. A., Eke, V., Frenk, C. S., Gao, L., Jenkins, A., Theuns, T., Wang, J., & White, S. D. M. 2012, *MNRAS*, 420, 2318
- Ludlow, A. D., Benítez-Llambay, A., Schaller, M., Theuns, T., Frenk, C. S., Bower, R., Schaye, J., Crain, R. A., *et al.* 2017, *Phys. Rev. Lett.*, 118, 161103
- Moore, B. 1994, *Nature*, 370, 629
- Navarro, J. F., Frenk, C. S., & White, S. D. M. 1996a, *ApJ*, 462, 563
- Navarro, J. F., Eke, V. R., & Frenk, C. S. 1996b, *MNRAS*, 283, L72
- Navarro, J. F., Frenk, C. S., & White, S. D. M. 1996a, *ApJ*, 490, 493
- Navarro, J. F., Benítez-Llambay, A., Fattahi, A., Frenk, C. S., Ludlow, A. D., Oman, K. A., Schaller, M., & Theuns, T. 2017, *MNRAS*, 471, 1841
- Oman, K. A., Navarro, J. F., Fattahi, A., Frenk, C. S., Sawala, T., White, S. D. M., Bower, R., Crain, R. A., *et al.* 2015, *MNRAS*, 452, 3650
- Oman, K. A., Navarro, J. F., Sales, L. V., Fattahi, A., Frenk, C. S., Sawala, T., Schaller, M., & White, S. D. M. 2016, *MNRAS*, 460, 3610
- Oman, K. A., Marasco, A., Navarro, J. F., Frenk, C. S., Schaye, J., & Benítez-Llambay, A. 2017a, *pre-print*, arXiv: 1706.07478
- Oman, K. A., Starkenburg, E., & Navarro, J. F. 2017b, in: Forbes, D. A. & Lopez, E. D. (eds.), *On the origin (and evolution) of baryonic galaxy halos*, *Galaxies*, 5, 33
- Pineda, J. C. B., Hayward, C. C., Springel, V., Mendes de Oliveira, C. 2017, *MNRAS*, 466, 63
- Pontzen, A., & Governato, F. 2014, *Nature*, 506, 171
- Read, J. I., & Gilmore, G. 2005, *MNRAS*, 356, 107
- Read, J. I., Iorio, G., Agertz, O., & Fraternali, F. 2016, *MNRAS*, 462, 3628
- Rhee, G., Valenzuela, O., Klypin, A., Holtzman, J., & Moorthy, B. 2004, *ApJ*, 617, 1059
- Sales, L. V., Navarro, J. F., Oman, K. A., Fattahi, A., Ferrero, I., Abadi, M., Bower, R., Crain, R. A., *et al.* 2017, *MNRAS*, 464, 2419
- Sawala, T., Frenk, C. S., Fattahi, A., Navarro, J. F., Bower, R. G., Crain, R. A., Dalla Vecchia, C., Furlong, M., *et al.* 2016, *MNRAS*, 457, 1931
- Sawala, T., Pihajoki, P., Johansson, P. H., Frenk, C. S., Navarro, J. F., Oman, K. A., & White, S. D. M. 2017, *MNRAS*, 467, 4383
- Schaye, J., Crain, R. A., Bower, R. G., Furlong, M., Schaller, M., Theuns, T., Dalla Vecchia, C., Frenk, C. S., *et al.* 2015, *MNRAS*, 446, 521
- Spergel, D. N., & Steinhardt, P. J. 2000, *Phys. Rev. Lett.*, 84, 3760
- Starkenburg, E., Oman, K. A., Navarro, J. F., Crain, R. A., Fattahi, A., Frenk, C. S., Sawala, T., & Schaye, J. 2017, *MNRAS*, 465, 2212
- Valenzuela, O., Rhee, G., Klypin, A., Governato, F., Stinson, G., Quinn, T., & Wadsley, J. 2007, *ApJ*, 657, 773
- Walter, F., Brinks, E., de Blok, W. J. G., Bigiel, F., Kennicutt, R. C., Jr, Thornley, M. D., Leroy, A. 2008, *AJ*, 136, 2563
- Wang, M.-Y., Fattahi, A., Cooper, A. P., Sawala, T., Strigari, L. E., Frenk, C. S., Navarro, J. F., Oman, K. A., *et al.* 2017, *MNRAS*, 468, 4887